Title: The absorption- and luminescence spectra of Mn3+ in beryl and vesuvianite

Author: Maria Czaja, Radosław Lisiecki, Artur Chrobak, Rafał Sitko, Zbigniew Mazurak

Citation style: Czaja Maria, Lisiecki Radosław, Chrobak Artur, Sitko Rafał, Mazurak Zbigniew. (2018). The absorption- and luminescence spectra of Mn3+ in beryl and vesuvianite. “Physics and Chemistry of Minerals” (Vol. 45, iss. 5 (2018), s. 475-488), doi 10.1007/s00269-017-0934-x

Physics and Chemistry of Minerals (2018) 45:475–488
https://doi.org/10.1007/s00269-017-0934-x

ORIGINAL PAPER

The absorption- and luminescence spectra of Mn^{3+} in beryl and vesuvianite

Maria Czaja[1] · Radosław Lisiecki[2] · Artur Chrobak[3] · Rafał Sitko[4] · Zbigniew Mazurak[5]

Received: 9 June 2017 / Accepted: 28 November 2017 / Published online: 8 December 2017

Abstract
The electron absorption-, photoluminescence- and electron paramagnetic-resonance spectra of Mn^{3+} in red beryl from Wah Wah Mountains (Utah USA) and of pink- and purple vesuvianite from Jeffrey Mine (Asbestos, Canada) were measured at room- and low temperatures. The crystal field stabilization energies are equal to 130.9 kJ/mol for the red beryl, and 151.5–158.0 and 168.0 kJ/mol for for the pink- and the purple vesuvianite, respectively. The red photoluminescence of Mn^{3+} was not intensive either at room- or at low temperatures. The high Mn content in the crystals caused the emergence of an additional emission band and short photoluminescence-decay lifetimes. The latter are only 183 μs for beryl and 17 μs for vesuvianite.

Keywords Mn^{3+} ion · Luminescence · Optical absorption · Beryl · Vesuvianite

Introduction

Mn^{3+} belongs to $3d^4$ electronic configurations, where the ground term ^5D is the only quintet term, whereas the other terms are triplets and singlets. In the octahedral crystal field, the ^5D term splits into the lower ^5Eg and upper $^5T_{2g}$ terms. The configurations of the lowest energy of the Mn^{3+} ion are: $^5E(^5D) - t_{2g}{}^3e_g$; $^5T_2(^5D) - t_{2g}{}^2e_g{}^2$; $^3T_1(^3H) - t_{2g}{}^4$; $^1T_2(^1I) - t_{2g}{}^4$; and $^1E(^1I) - t_{2g}{}^4$ (Sugano et al. 1970; Powell 1998). The energy level diagram of d^4 ions is presented in Fig. 1. Splitting of the ground ^5D term can be intensified or induced by the Jahn–Teller effect of transition metal ions. The distinct Jahn–Teller effect causes the d^4 ion to occupy a crystal site of symmetry lower than octahedral. As a result, in many natural- and synthetic Mn^{3+}-bearing crystals, the site symmetry is reduced tetragonal (Burns and Strens 1967; Hålenius 1978) or monoclinic (Hålenius 2004). The scheme of the ground- and first-excited states of the d^4 ion in different symmetry sites is sketched in Fig. 2. As only the ^5E level has a configuration with one non-paired electron, the Jahn–Teller stabilization energy for this level is expected to be the highest. For the other levels, smaller stabilization energies are expected.

The optical absorption spectrum of Mn^{3+} consists of an intensive, broad, often two-humped band due to $^5E_g \rightarrow {}^5T_{2g}$ transition with Jahn–Teller splitting of the $^5T_{2g}$ level or of two dichroic bands in the lower symmetry fields. On the short-wavelength side of this main $^5E_g \rightarrow {}^5T_{2g}$ absorption band, a characteristic deep feature is observed in some cases. It is attributed to a Fano-antiresonance effect between the ^3E and the $^5T_2$ levels. With increasing crystal field strength, a shift of absorbance band towards shorter wavelengths is observed and splitting of upper-level e_g orbitals is measured in the red- or NIR range of the spectrum (Kück et al. 1998b; Gaft et al. 2011). The less frequent spin-forbidden transitions $^5E_g \rightarrow {}^3T_{1g}(^3H)$ and $^5E_g \rightarrow {}^3E_g(^3H)$ may be measured as narrow lines.

Mn^{3+} is a mineral component that can be responsible for a red to violet or pink color on the one hand and yellow or green and blue on the other. The absorption spectra of Mn^{3+}-bearing minerals have been measured for grossular

✉ Maria Czaja
maria.czaja@us.edu.pl

1 Faculty of Earth Sciences, University of Silesia, Będzińska 60, 41-200 Sosnowiec, Poland

2 Institute of Low Temperature and Structure Research, Polish Academy of Sciences, Okólna 2, 50-422 Wrocław, Poland

3 Insitute of Physics, Silesian University, Uniwersytecka 4, 40-003 Katowice, Poland

4 Institute of Chemistry, Silesian University, Szkolna 9, 40-003 Katowice, Poland

5 Center of Polymer and Carbon Materials, Polish Academy of Sciences, ul. M. Skłodowskiej-Curie 34, 41-819 Zabrze, Poland

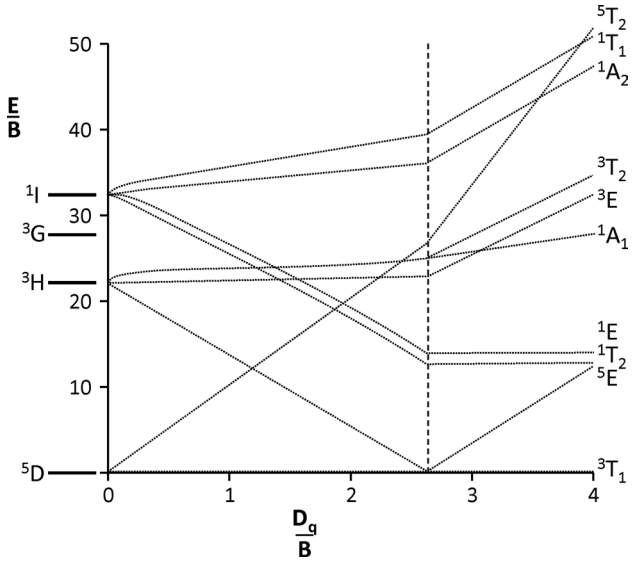

Fig. 1 Simplified sketch of the Tanabe–Sugano diagram for a d^4 electron configuration in octahedral symmetry

(Gaft et al. 2013), Mn-hydrogarnets (Hålenius 2004), Mn-andalusite and kyanite (Abs-Wurmbach et al. 1977; Hålenius 1978; Kai et al. 1980; Smith et al. 1982; Langer et al. 1982; Abu-Eid et al. 1978; Gaft et al. 2011), yoderite (Langer et al. 1982), orthozoisite and clinozoisite (Langer et al. 2002), rhodonite (Paião and Watanabe 2008), epidote (Smith et al. 1982; Burns and Strens 1967), vesuvianite (Platonov et al. 1995; Panikorovskii et al. 2017), beryl (Nassau and Wood 1968; Fridrichova et al. 2017), diopside (Hålenius and Skogby 1996), clinopyroxene and amphiboles (Ghose et al. 1986), montmorillonite (Sherman and Vergo 1988), chlorite (Hålenius 1984) and tourmaline (Smith 1978). The polarized- or un-polarized spectra measured for red- and purple crystals contain the main $^5E_g \rightarrow {}^5T_{2g}$ transition band at 535–565 nm. In contrast, the spectra recorded for yellow- or green crystals comprise two bands at 450 and 630 nm. The crystal-field splitting 10Dq for Mn-bearing minerals collected by Burns (1993) varies from 19,800 cm^{-1} for garnet to 12,800 cm^{-1} for tourmaline. Lower 10Dq values have been calculated for blanfordite (11,650 cm^{-1}), winchite (11,640 cm^{-1}), juddite (11,925 cm^{-1}) and montmorillonite (12,999 cm^{-1}). The Mn^{3+} crystal-site symmetries in these minerals are usually lower than octahedral and estimated to be tetragonal (D_{4h} in andalusite, epidote and beryl, C_{4v} in vesuvianite, montmorillonite), trygonal (D_{3h} in yoderite) or monoclinic C_{2v} in andalusite, Mn-hydrogarnet and hentitermierite, C_2 in amphiboles and beryl (after Chithambo et al. 1995).

The luminescence spectra of Mn^{3+} ions in minerals and synthetic materials have been rarely measured. A strong Jahn–Teller effect introduces various channels for non-radiative relaxation and the quenching of manganese luminescence. The intensive Mn^{3+} luminescence at room- and low temperatures was measured only by Kück et al. (1998b, c) for Mn^{3+}-doped garnets $Y_3Al_2O_{12}$ (YAG), $Y_3Ga_5O_{12}$ (YGG), $Gd_3Ga_5O_{12}$(GGG), $Y_3Sc_2Ga_3O_{12}$ (YSGG) and $Gd_3Sc_2Ga_3O_{12}$ (GSGG). At room temperature, the two spin-allowed transitions $^5T_2$–$^5E'$, $^5E''$ were observed as bands at 620–659 nm and 758–842 nm. At low temperatures, only the $^1T_2$ level is thermally populated. At $T = 12$K, two broad bands ($^1T_2 \rightarrow {}^5E', {}^5E''$) with maxima at 14,300 cm^{-1} (700 nm) and 11,700 cm^{-1} (850 nm), as well as a structured band around 9000 cm^{-1} (1100 nm, $^1T_2 \rightarrow {}^3T_2$), were measured. The decay times at $T = 12$ K are a few milliseconds while, at higher temperatures, lifetimes decrease to ca 0.5 µs. Moreover, the Mn^{3+} luminescence of $YMnO_3$ (Takahashi et al. 2002) and $ZnAl_2O_4$ (Cornu et al. 2014) are known.

Unlike that of Mn^{2+}, Mn^{3+} luminescence is not well known in minerals. Mn^{3+} emission was reported recently in orange Mn-containing kyanite (Gaft et al. 2011) and in grossular (Gaft et al. 2013). A broad luminescence band was detected under excitation at 355 nm at $T = 300$ K in orange kyanite with a maximum at 765 nm and a long decay time of 830 µs (Gaft et al. 2011). This red band disappeared at 77 K. In our opinion, this emission should originate from the $^5T \rightarrow {}^5E$ transition. Using a time-resolved procedure, Gaft et al. (2013) measured a broad emission band at 653 nm at room temperature ($G = 50$µs, $D = 100$ ns) in natural grossular from Mexico. This emission was split at $T = 100$ K into two bands at 633 and 698 nm. The nature of the double emission peak has not been explained. Mn^{3+} (and Mn^{2+}, Cr^{3+} and Mn^{4+}) luminescence has been noted in yellow sapphires (Palanza et al. 2010). For beryl, only thermoluminescence measurements have been made (Chithambo et al. 1995). To

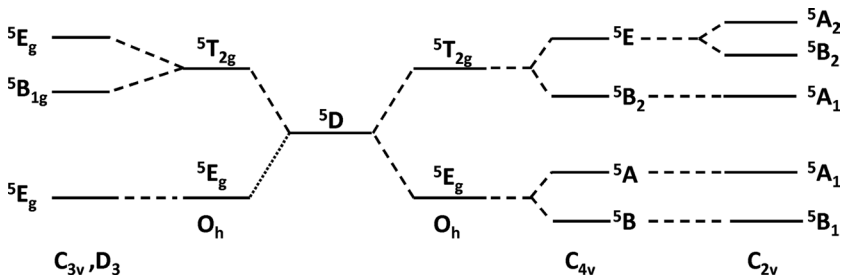

Fig. 2 Schematic energy level diagram for Mn^{3+} in octahedral fields of descending symmetry

date, no photoluminescence in Mn^{3+}-vesuvianite or beryl has been reported.

Ultrafast laser spectroscopy is a spectroscopic technique that uses ultrashort pulse lasers in the study of dynamics on extremely short timescales. Compared with continuous wave (CW) and long-pulse lasers, the femtosecond laser may induce different phenomena when it interacts with matter. No case of the application the ultrashort excitation in studies of the luminescence properties of minerals is known to us. For the crystals studied in this work, some competitive effects to CW measurements can be expected. Among them, an alternative way of Mn^{3+} luminescence excitation is recognized and/or the possibility of short-lived point-defect emission.

Materials and methods

The red beryl studied in this work was extracted from cavities in rhyolite from the Wah Wah Mountains, Beaver County, Utah, USA (Wood and Nassau 1968). The crystal is a flat pinacoid {001} up to 15 mm across and 14 mm thick. The purple- and pink vesuvianite crystals studied by us, and the green variety of vesuvianite, are from the asbestos chrysotile Jeffrey Mine (Asbestos, Canada). The crystals are tetragonal prisms elongated parallel to the *Z*-axis. They are often variously colored with zones of deep purple (lilac) or pink and yellow. Several small crystals (2 × 2 × 7 mm) were chosen which, in so far as was possible, were homogenous deep purple- or pink colored (magenta). Several grains of these minerals were selected for electron microprobe analysis. Powdered samples (0.2 g) were prepared for chemical analyses and EPR measurements. Fragments of vesuvianite crystals of similar color to those measured by electron absorption spectrophotometer, and which exhibited orange luminescence, were selected.

Chemical analyses

The major chemical constituents of the crystals were determined using an electron-microprobe analyzer (CAMECA sx100; 15 kV, 40–50 nA). The following lines and standards were used: Ca*Kα*, Si*Kα*, Mg*Kα* (diopside). Ti*Kα* (rutile), Al*Kα* (orthoclase), Fe*Kα* (Fe_2O_3). Mn*Kα* (rhodochrosite). Corrections were made using the PAP procedure provided by CAMECA. The results calculated for an average of 5 measuring points are presented in Table 1. Chemical analyses were performed using an Epsilon 3 (Panalytical, Almelo, Netherlands) energy-dispersive X-ray fluorescence (EDXRF) spectrometer with a Rh target X-ray tube operated at a maximum voltage of 30 keV and a maximum power of 9 W. The spectrometer is equipped with a thermoelectrically-cooled silicon drift detector (SDD) with an 8-µm Be window and a resolution of 135 eV at 5.9 keV. Quantitative analysis was performed using Omnian software based on a fundamental parameter method and under the following measurement conditions: 12 kV, 300 s counting time, helium atmosphere, 50-µm Al primary beam filter for Ti and Cs; 20 kV, 120 s counting time, air atmosphere, 200-µm Al primary beam filter for Mn and Fe; 30 kV, 120 s counting time, air atmosphere, 100-µm Ag primary beam filter for Cu, Zn, Ga, As, Rb, Sr, Y, Zr, Nb, Th and U. The current of the X-ray tube was fixed so as not to exceed a dead-time loss of ca 50%. The results are presented in Table 1.

Table 1 The chemical composition of the studied crystals

Compound	Red beryl	Purple vesuvianite	Pink vesuvianite
Major chemical constituents [wt%] ASA MC-			
SiO_2	65.10	36.8	36.8
TiO_2	0.30	0.09	0.04
Al_2O_3	16.08	15.15	1500
Mn_2O_3	1.52	1.17	2.09
Fe_2O_3	4.20	0.61	0.59
Cr_2O_3	0.00	0.40	0.50
MgO	0.20	5.52	3.42
CaO	0.00	36.70	36.70
BeO[a]	12.60	0.00	0.00
Trace elements content from X-ray fluorescence [wt%]			
Mn	0.53 ± 0.034	0.41 ± 0.038	0.73 ± 0.037
Fe	1.47 ± 0.22	0.212 ± 0.036	0.207 ± 0.037
Trace element content from X-ray fluorescence [ppm]			
Ti	2,250 ± 150	691 ± 40	222 ± 12
Cu	30 ± 2.0	4.8 ± 0.25	4.7 ± 0.26
Zn	0.11 ± 0.013	110 ± 6.9	284 ± 17
Ga	104 ± 6.8	9.1 ± 0.55	–
As	6.5 ± 0.42	–	–
Rb	928 ± 44	–	–
Sr	–	45 ± 2.7	27 ± 2.0
Y	–	21 ± 1.3	–
Zr	184 ± 9.8	74 ± 4.1	46 ± 3.5
Nb	47 ± 3.0	–	–
Cs	0.41 ± 0.035	–	–
Th	–	11.6 ± 0.68	–
U	146 ± 8.5	–	–

[a]Calcultaed to close sum to 100%

Electron absorption and photoluminescence spectroscopy

Absorption spectra of the red beryl and of the purple- and pink vesuvianite were measured at room- and low (7 K) temperatures using a Cary-Varian Model 2300 spectrophotometer in the spectral range from 2000 nm (5000 cm^{-1}) to

340 nm (30,000 cm^{-1}). The beryl sample was placed with its *Z*-axis parallel to the propagating light and a ω (σ) spectrum recorded.

Electron absorption measurements were made at room- and low (7 K) temperatures for several vesuvianite specimens. The polarized absorption spectra were obtained for polarization parallel to and perpendicular to the *Z*-axis. Additionally, the spectra were measured at low (7 K) temperature. As the absorption bands were weak, measurements at low temperatures increased the possibility of clearly distinguishing all absorption transitions.

Steady time-luminescence spectra of the studied samples were obtained using a Jobin–Yvon (SPEX) FLUORLOG 3–12 spectrofluorimeter at room temperature with a 450W xenon lamp, a double-grating monochromator and a Hamamatsu 928 photomultiplier. Measurements at low temperature were made using a Physik LPD3000 laser (pumped by a Lambda Physik LPX100 excimer laser). Some of the luminescence spectra were recorded using a Dongwoo Optron DM 158i excitation monochromator and a DM711 emission monochromator with a 750 mm focal length. An ozone-free Xenon lamp DL 80-Xe and diode lasers were the excitation sources.

Some emission experiments involved an excitation source comprising a femtosecond laser (CoherentModel "Libra") coupled to an optical parametric amplifier (LightConversionModel "OPerA"). The source delivers 100 fs pulses at a repetition rate regulated up to 1 kHz at a wavelength tuned between 230 and 2800 nm. The pulse energy is 6–150 µJ, depending on the spectral region. The excitation light was focused on the single crystals using a lens with a focal length of 15 cm.

Luminescence decay curves were measured using pulsed excitation delivered by a Continuum Surelite optical parametric oscillator (OPO) pumped with the third harmonic of an Nd:YAG laser. The decays were measured with a Hamamatsu R-955 photomultiplier connected to a Tektronix Model TDS 3052 digital oscilloscope. For low-temperature measurements, samples were placed in a continuous-flow liquid-helium cryostat equipped with a temperature controller.

Electron paramagnetic measurements

Electron paramagnetic resonance (EPR) spectra were obtained using a X-band spectrometer with a TE 011 rectangular cavity and 100 kHz field modulation. The magnetic field induction ranged from 0.06 to 0.4 T (at room temperature). The microwave frequency was measured using a Hewlett Packard 534 microwave frequency counter.

Results and discussion

Absorption spectra

In beryl (ideal formula $Be_3Al_2[Si_6O_{18}]$) crystals, the manganese (Mn^{2+}) ions occupy Al^{3+} sites (Artioli et al. 1993) of O_h site symmetry though trigonal C_{3v} symmetry may be expected, as for Cr^{3+} in emerald. The (Al,Mn)-O distance is 1.916 Å. For red beryl from the Wah Wah Mts, Nassau and Wood (1968) showed bands Mn^{3+} bands at 480 and 510 nm for perpendicular polarization and, for parallel polarization, at 545 nm. Other absorption bands appearing at 480 and 380 nm are recognized as due to the presence of Fe^{3+} (Wood and Nassau 1968). On the spectrum of red beryl from the same locality measured for parallel polarization at 6K, and published on the Caltech internet page (http://minerals.gps.caltech.edu/FILES/Visible/Beryl/be602.gif), an intensive non-symmetrical absorption band with a maximum at 560 nm and a sharp line at 430 nm appear.

For beryl crystal from Utah, Fridrichová et al. (2017) allowed the possibility of tetragonal distortion of the crystal site of the Mn^{3+} ion. They recognized the band at ~7190 cm^{-1} as reflecting transition among ^5B and ^5A sublevels of the ground ^5E level in the case of such tetragonal distortion. However, the possibility that this band may come from water molecules was rejected by them. The

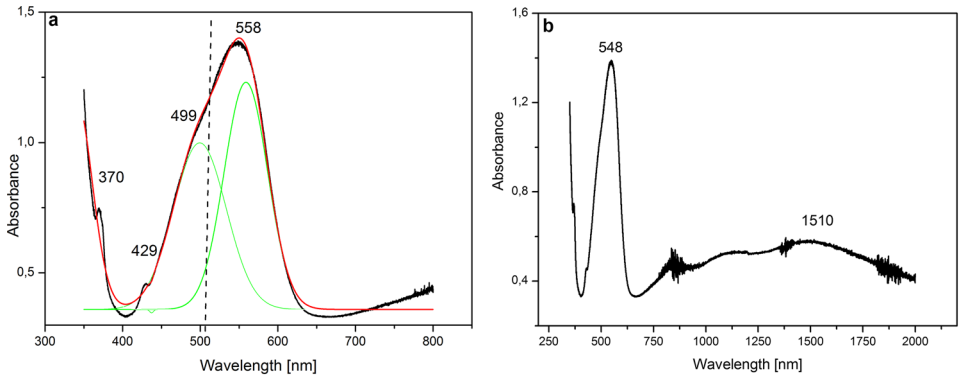

Fig. 3 Absorption spectra of red beryl: **a** $T = 7$K; **b** $T = 300$ K

spectroscopic parameters were obtained as follows: the crystal-field parameters D_q as 1770 cm^{-1}, tetragonal field parameters D_t and D_s as 515 and 1150 cm^{-1}, respectively and the Racah parameter B as 835 cm^{-1}. The crystal studied by Fridrichová et al. (2017) contains, on average, 6 times less Mn than the crystal studied by us.

The absorption spectra of the beryl, measured at low temperature and for parallel polarization, are shown in Fig. 3a. At low temperature (7 K), the 548 nm band splits to 499 nm (20,040 cm^{-1}) and 558 nm (17,921 cm^{-1}) lines corresponding to two spin-allowed transitions from the Jahn–Teller split ^5E ground state to the $^5T_2$ level. The splitting is equal to 2119 cm^{-1}. From the energy of the $^5E \rightarrow {}^5T_2$ absorption band maximum, the crystal-field parameter D_q is determined as 1825 cm^{-1}. The Crystal Field Stabilization Energy (CSFE) for Mn^{3+} ions in this crystal is $\frac{3}{5} \cdot 10 \cdot D_q = 10,950$ cm^{-1} i.e., 130.9 kJ/mol. On the short-wavelength side of this main absorption band, a characteristic feature in the form of a deep is observed which is attributed to a Fano-antiresonance effect (at 511 nm) between the ^3E and the $^5T_2$ levels. This Fano antiresonance effect is caused by the mixing between spin–orbit components of these levels and it is attained at the crossing of a spin-forbidden, crystal-field independent term with a spin-allowed, crystal-field-dependent term. Accordingly, the ratio between the crystal-field strength D_q and the Racah parameter B was roughly estimated to be $D_q/B \approx 2.23$ and, thus, the Racah parameter B should be estimated as 818 cm^{-1}. Moreover, two very sharp lines at 370 nm (27.027 cm^{-1}) and 429 nm (23,310 cm^{-1}) may be associated with $^5E \rightarrow {}^3A_1(^3F)$ and $^5E \rightarrow {}^3T_2(^3H)$ transitions, respectively. In NIR, a broad and weak absorption at 1510 nm (6622 cm^{-1}) is also observed (Fig. 3b). It can be assigned to a transition between sublevels of ground ^5E level $^5E' \rightarrow {}^5E''$. This band may also be due to an overtone of water-molecule vibration.

Panikorovskii et al. (2017) proposed the following formula for different vesuvianite-group minerals: $X_{18}X4Y1Y2_4Y3_8T_{0\text{-}5}(Z_2O_7)_4[(ZO_4)_{10-x}(H_4O_4)_x](W)_9O_{1-3}$, where $x < 3$, X are seven- to nine-coordinated sites (Ca, Na, K, Fe^{2+}, REE), X4 has a square antiprism coordination (Ca, Na), Y1 has a square pyramidal coordination (Fe^{3+}, Mg, Al, Fe^{2+}, Cu^{2+}), Y2 and Y3 have octahedral coordination (Al, Mg, Zn, Fe^{2+}, Fe^{3+}, Mn^{2+}, Mn^{3+}, Ti, Cr, Zn), T (B, Fe) is the additional site with triangular- and tetrahedral coordination, ZO_4 (Si, H_4O_4) and Z_2O_7 are ortho-and di-orthosilicate groups, respectively, and W=OH, F, Cl and minor O.

The crystal structure of the Mn-bearing vesuvianite from the Asbestos deposit was refined by Fitzgerald et al. (1986) who determined the chemical formula to be $(Ca_{18.68}Mn_{0.06}Mg_{0.26})Al_4Al(Al_{6.51}Mg_{1.49})(Si_{17.49}Al_{0.51})O_{69}(OH)_{9.0}$. Armbruster and Gnoss (2000) and Armbruster et al. (2000) also proved that, in manganvesuvianite $Ca_{19}Mn^{3+}(Al,Mn^{3+},Fe^{3+})_{10}(Mg,Mn^{2+})_2Si_{18}O_{69}(OH)_9$ from the N'chwanignig II mine manganese deposit (South Africa), Mn as Mn^{3+} mainly prefers the Y1 site with five-fold coordination rather than the sixfold coordination of Y3 or Y2 sites. The metal–ligand distances for Y1 sites (C_{4v} site symmetry) are larger than for Y3 and Y2 which have lower symmetry, most probably C_{2v}.

Płatonov et al. (1995) have measured optical absorption spectra for yellow-, pink- and lilac vesuvianites from Lower Silesia (Poland) using a microscope spectrometer with perpendicular- and parallel polarization. Their samples were prepared as thin slabs from crystallites (< 1–10 mm). For perpendicular polarization, only one strong band was measured for both the yellow vesuvianite at 23,600 cm^{-1} (424 nm) and for the lilac variety at 18,500 cm^{-1} (540 nm), but, for the pink crystal, two bands were observed at 23,100 and 18,500 cm^{-1}. They proposed, that, in yellow vesuvianite, Mn^{3+} ions are accommodated in five-fold coordinated sites with C_{4v} symmetry and, in lilac vesuvianite, in AlFe-octahedra with C_{2v} symmetry, while in pink vesuvianite in both type of sites. Because metal–ligand distances for Y1 sites are larger than for Y2,3 sites, the absorption band at 18,500 cm^{-1} should be assigned to these sites. However, Płatonov et al. (1995) claimed that the crystal-field force distinctly increases for C_{4v} symmetry sites due to the Jahn–Teller effect. This conclusion may need verification as it is inconsistent with the relation between metal–ligand distance and crystal field splitting $10D_q \sim \frac{1}{(\text{metal-ligand distance})^5}$. In addition, a crystal field with symmetry lower than tetragonal also strengthens the Jahn–Teller effect.

Other absorption spectra for purple vesuvianites are given on the website of The California Institute of Technology (http://minerals.gps.caltech.edu). For purple vesuvianite from the Jeffrey Mine (Asbesos, Canada), the following bands appear: for perpendicular polarization intensive bands at 425 nm (23,530 cm^{-1}) and 610 nm (16,400 cm^{-1}) and for parallel polarization weak absorption band at 450 nm (22,222 cm^{-1}) and 517 nm (19,340 cm^{-1}). (http://minerals.gps.caltech.edu/FILES/Visible/vesuvianite/Vesuvianite%201079,%20Quebec-2.39%20mm.gif). For a deep purple crystal from the N'chwaniging II mine (South Africa), for perpendicular polarization, an intensive band at 550 nm (18,180 cm^{-1}) was measured (http://minerals.gps.caltech.edu/FILES/Visible/vesuvianite/Vesuvianite%201932%20N%27chwaning%20-%2019um.jpg), and for a purplish-green vesuvianite from Paraiba (Brazil), two bands at 520 nm (19,230 cm^{-1}) and 700 nm (14,285 cm^{-1}) (http://minerals.gps.caltech.edu/FILES/Visible/vesuvianite/Vessuvianite%20Paraiba%202907%204.27mm.gif) that were probably from Mn^{3+} and Cr^{3+} ions.

Panikorovskii et al. (2017) presented cyprine $Ca_{19}Cu^{2+}(Al,Mg,Mn)_{12}Si_{18}O_{69}(OH)_9$, for which in two

zones, chromium, manganese iron and copper are present in different crystal sites. The absorption band at 15,400 cm^{-1} (~650 nm) was attributed to d-d transition of Cu^{2+} ion.

The authors claimed that the five-coordinated C_{4v} position was completely occupied by Cu^{2+} ions, whereas Mn^{3+} and other ions occupied other sites. The other bands (23,500, 21,100, 20,000, 18,000 and 12,000 cm^{-1}) are associated with the Mn^{3+} transitions.

The polarized optical spectra of purple- and pink Mn-vesuvianite from the Jeffrey Mine measured at $T=7$ K are shown in Fig. 4a–c. Very sharp absorption line at 462 nm (21,650 cm^{-1}) is associated with $^5E \rightarrow {}^3T_2(^3H)$ transition.

For the purple vesuvianite, the following bands and transitions are identified:

- $^5B_{1g}(^5E) \rightarrow {}^5A_{1g}(^5E)$—1464 nm, i.e., 6350 cm^{-1}, for E||c and E⊥c polarization,
- $^5B_{1g}(^5E) \rightarrow {}^5B_{2g}(^5T_{2g})$—516 nm, i.e., 19,380 cm^{-1}, for E⊥c polarization,
- $^5B_{1g}(^5E) \rightarrow {}^5E_g(^5T_{2g})$—446 nm, i.e., 22,422 cm^{-1}, for E||c polarization.

It is proposed here that these transitions relate to Mn^{3+} in the crystal sites Y1 with C_{4v} symmetry. The transitions in the tetragonal field are described by the following equations:

$$^5B_{1g}(^5E) \rightarrow {}^5A_{1g}(^5E) = 4 \cdot D_s + 5 \cdot D_t$$
$$^5B_{2g}(^5E) \rightarrow {}^5B_{2g}(^5T_2) = 10 \cdot D_q$$
$$B_{1g}(^5E) \rightarrow {}^5E_g(^5T_2) = 3 \cdot D_s - 5 \cdot D_t + 10 \cdot D_q$$

D_t and D_s are tetragonal field parameters. An axial elongation is indicated by the same sign, an axial compression by opposite signs. The Crystal Field Stabilization Energy (CFSE) equals $\frac{3}{5} \cdot 10 \cdot D_q + \frac{1}{2}(4 \cdot D_s + 5 \cdot D_t)$. For purple vesuvianite, $10D_q = 19{,}380$ cm^{-1}, $D_s = 1410$ cm^{-1} and $D_t = 238$ cm^{-1}. The Racah parameter $B = 760$ cm^{-1} and CFSE = 15,043 cm^{-1}, i.e., 168 kJ/mol were also determined.

As Mn^{3+} ions occupy other octahedral crystal sites (most probably with C_{2v} symmetry) in the pink vesuvianite, the following transitions can be recognized:

- $^5B_1(^5E) \rightarrow {}^5A_1(^5E)$—1460 nm, i.e., 6850 cm^{-1}, for E||c and E⊥c polarization,

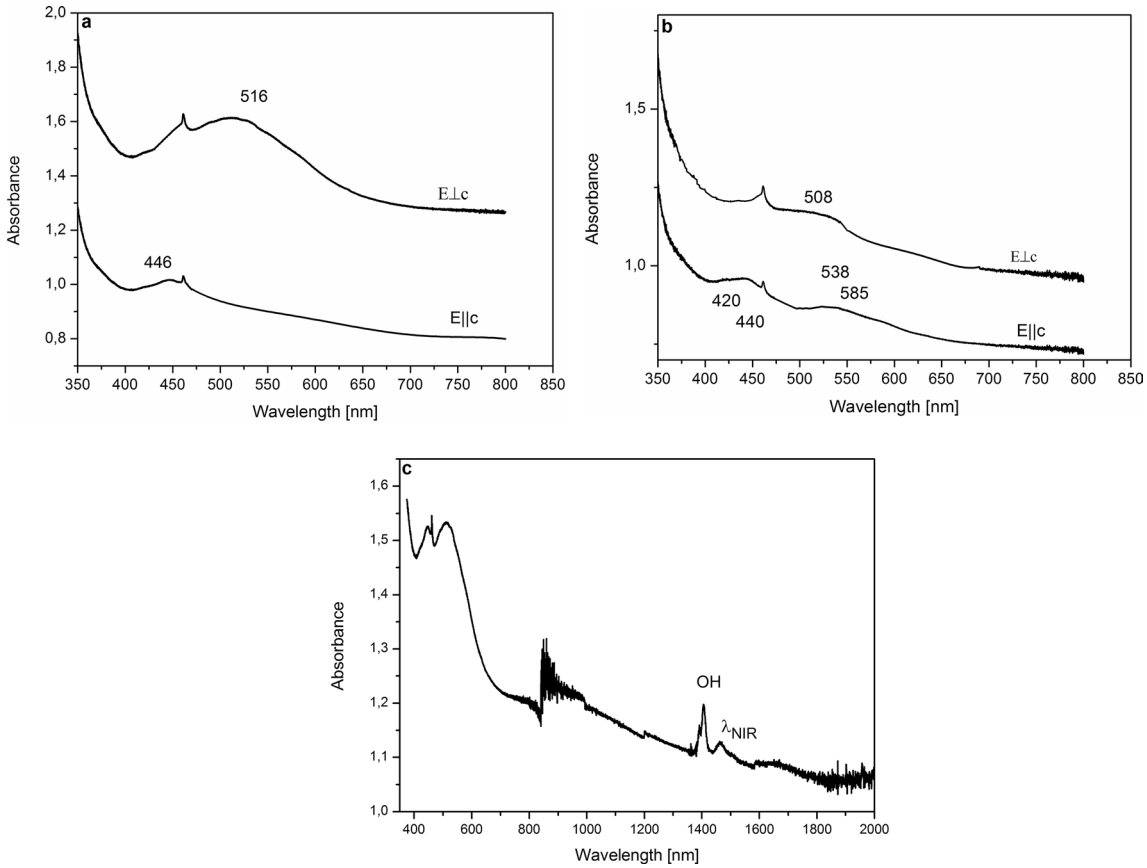

Fig. 4 **a** Absorption spectra of purple vesuvianite crystal measured at $T=7$ K. **b** Absorption spectra of pink vesuvianite crystal measured at $T=7$ K. **c** Absorption spectrum of purple vesuvianite in Vis–NIR region at $T=7$ K

- $^5B_1(^5E) \rightarrow {}^5A_2(^5T_2)$—440 nm, i.e., 22,727 cm^{-1} and 420 nm, i.e., 23,810 cm^{-1}, for E||c polarization,
- $^5B_1(^5E) \rightarrow {}^5B_2(^5T_2)$—508 nm, i.e., 19,685 cm^{-1}, for E⊥c polarization,
- $^5B_1(^5E) \rightarrow {}^5A_1(^5T_2)$—538 nm, i.e., 18,315 cm^{-1} and 585 nm, i.e., 17,094 cm^{-1}, for E||c polarization.

In addition, since the bands of ^5B (^5E) → $^5A_2(^5T_2)$ and $^5B_1(^5E) \rightarrow {}^5B_2(^5T_2)$ transition looks double, it is possible that the absorbance was measured for two sites—most probably Y2 and Y3. If yes,

$$10 \cdot D_q = \frac{1}{3}[E(^5B_1(^5E) \rightarrow {}^5A_2(^5T_2)) + E(^5B_1(^5E) \rightarrow {}^5B_2(^5T_2)) + E(^5B_1(^5E) \rightarrow {}^5A_1(^5T_2))] - \frac{1}{2}E(^5B_1(^5E) \rightarrow {}^5A_1(^5E)$$

Thus, $10D_q = 17{,}118$ cm^{-1} and CFSE = 13,225 cm^{-1}, i.e., 158.3 kJ/mol for the one site and $10D_q = 16{,}410$ cm^{-1} and CFSE = 12,678 cm^{-1}, i.e., 151.7 kJ/mol for the second site. The Racah parameter $B = 760$ cm^{-1}. The character of the Mn^{3+}–O bond in vesuvianite crystals is more covalent than in beryllium, as their Racah parameter B (760 cm^{-1}) is lower than that of berylium crystals.

The absorption band at 12,500 cm^{-1} (800 nm) measured by Platonov et al. (1995) and Panikoroskii et al. (2017) could be recognized as transition $^5A_{1g} \rightarrow {}^5E_g(^5T_{2g})$. However, at low temperature, this level is depopulated and the transition $^5A_{1g} \rightarrow {}^5E_g(^5T_{2g})$ cannot occur. Thus, the band corresponding to it cannot appear on the absorption spectra measured at low temperature (Fig. 4a, b).

The current results are not in conflict with those of Panikorovskii et al. (2017). The amounts of Mn in the cyprine vesuvianite crystal are greater for zones 2 than for zones 1.

(Panikorovkii et al. 2017), as they are for the pink variety compared to the purple variety in this study, although the polarization of bands of the pink vesuvianite spectrum (Fig. 4b) and those of zone 2 (Panikorovskii et al. 2017) is different. Moreover, the positions of the vesuvianite absorption bands measured by us differ to some extent from those measured by Płatonow et al. (1995) and Panikorovskii et al. (2017). This may be due to a difference in chemical composition, interaction of cations from the second coordination pile and Mn–Mn interaction, as indicated by luminescence measurements.

The comparison of CFSE values for the red beryl and for two crystal sites in the vesuvianite structure supports our interpretation that Mn^{3+} prefers the more distorted sites, not only those with tetragonal symmetry.

The values of the D_q parameter for the crystals studied in this paper do not depend only on the average Mn–O distance but also on the distortion of the crystal sites. Comparison of our results with those in the references cited earlier (Abs-Wurmbach et al. 1977; Ghose et al. 1986; Sherman and Vergo 1988; Platonov et al. 1995; Gaft et al. 2011; Fridrichová et al. 2017; Panikorovskii et al. 2017) can indicate that for crystal sites with symmetry lower than axial and for which OH groups could also be ligands (Mn-monmorrillonite, amphibole, henritermierite, epidote and pink vesuvianite), the Dq parameter varies according to a known relationship $D_q \sim r\,(\text{Mn–O, OH})^{-1}$. The remaining crystals do not exhibit the same relationship. For example, beryl has one of the smallest Mn–O distances and Dq is not the largest. The cause of this apparent incompatibility is the Jahn–Teller effect, which may be stronger and weaker for the same ion even in the same type of structure, as Kück et al. (1998a, c) has shown for the garnet series. Thus, this problem seems not to be so simple, and the influence of the second coordination zone or different covalent content of the chemical bond should be considered. First of all, much more data is necessary. Our results show the dependence of the Dq parameter on the deformation of the lattice site.

Emission spectra

Emission spectra for the red beryl crystal at room- and low (7K) temperature are shown in Fig. 5. At room temperature, intensive emission bands of the $^5T_2 \rightarrow {}^5E'$ transition at 630 nm (15,873 cm^{-1}) and of the $^5T_2 \rightarrow {}^5E''$ transition at 823 nm (12,150 cm^{-1}) were recorded. The decay time of the 630 nm emission at T = 300K is very short − 0.6 µs. These emission bands can be related to transitions from the $^5T_2$ level to two sublevels of the ground ^5E state. Femtosecond excitation led to no further luminescence bands.

At low temperature, the double-structured emission band has maxima at 617 and 674 nm and another other weak band at 810 nm. The luminescence lifetime of the 617 nm line is 15 µs, but that of 674 nm is 183 µs; the luminescence decay curves are single exponential. The emission bands at 674 and 810 nm originate from the $^1T_2 \rightarrow {}^5E$ transition. For this red beryl, no luminescence from Mn^{4+} or Cr^{3+} was noted (see Kück et al. 1998a). With femtosecond excitation, a single-emission band at 669 nm appears. Results of calculations of Jahn–Teller stabilization energies for the ^5E, $^5T_2$ and $^1T_2$ levels (Tables 2, 3, 4) show that these are as those for Mn^{3+}-doped garnets measured by Kück et al. (1998a), but the most significant difference is the much shorter luminescence-decay time at low temperature.

It has been assumed that the origin of the band at 617 nm may be due to (a) $^5T_2 \rightarrow {}^5E$ transition, (b) transition from

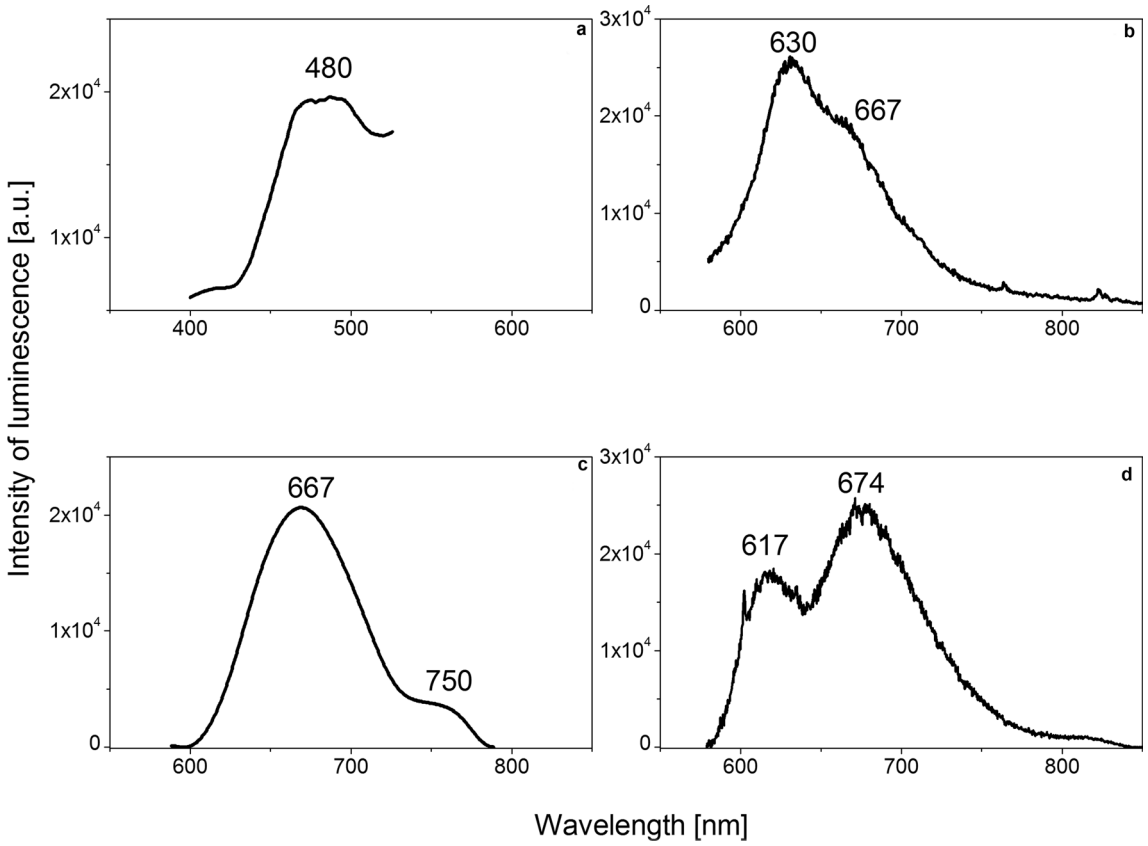

Fig. 5 Photoluminescence spectra of red beryl: **a** Excitation spectrum for $\lambda_{em} = 630$ nm at $T = 300$ K; **b** emission spectrum at $T = 300$ K and under xenon lamp excitation $\lambda_{ex} = 480$ nm; **c** emission spectrum at $T = 300$ K under laser excitation $\lambda_{ex} = 445$ nm; **d** emission spectrum at $T = 7$ K under laser excitation $\lambda_{ex} = 445$ nm

Table 2 The Jahn–Teller stabilization energies of ground level ^{5}E of studied crystals

Spectroscopic parameters	Crystal				
	Unit	Red beryl	GSGG/YAG[a]	Pink vesuvianite	Purple vesuvianite
Absorbance					
λ_{VIS}	[nm]	548	524/510	435	516
D_q	[cm^{-1}]	1825	1908/1960	1712/1641	1938
λ_{IR}	[nm]	1510	1361/1389	1460	1464
E_{NIR}	[cm^{-1}]	6622	7350/7200	6850	6830
$\Delta E_{JT}(^5E)$	[cm^{-1}]	1655	1838/1800	1712	1708
$\Delta E_{JT}(^5E) = \frac{E_{NIR}}{4}$					

two sublevels of the $^1T_2$ state which was split or (c) $^1E \rightarrow {}^5E$ transition. All such explanations based on a single-emission center should be rejected, as the energy difference between 617 and 674 nm centers is equal to 1370 cm^{-1}. The width of the 617 nm band is much smaller (855 cm^{-1}) than that of the 674 nm band (1459 cm^{-1}).

At low temperature, the probability of the higher state being populated is proportional to $\exp(-\Delta E/kT)$. This implies that the emission observed at 617 nm is due to a luminescence center other than the Mn^{3+} ion. A plausible reason for this emission is that it comes from Mn^{2+} ions present in octahedral sites. Gaft et al. (2013) have reported the 605 nm emission band of Mn^{2+} beside the emission band at 653 nm of Mn^{3+} for a grossular. EPR measurements show that in the red beryl being discussed here, Mn^{2+} ions are absent. The luminescence-decay time of 17 μs is too short

Table 3 The Jahn–Teller stabilization energies of excited level $^5T_2$ of studied crystals

Spectroscopic parameters	Crystal		
	Unit	Red beryl	GSGG/YAG[a]
Emission at 300 K			
$\lambda_1\ ^5T_2 \rightarrow\ ^5E'$	[nm]	628	659/620
E_1	[cm^{-1}]	15,798	15,167/16,143
$\lambda_2\ ^5T_2 \rightarrow\ ^5E''$	[nm]	823	842/758
E_2	[cm^{-1}]	12,150	11,884/13,199
τ	[μs]	0.6	< 0.5/1,110
$\Delta E(^5T_2)$	[cm^{-1}]	3774	3283/2944
$\Delta E_{JT}(^5T_2)$	[cm^{-1}]	538	366/301
$\Delta E_{JT}(^5T_2) = \frac{(\Delta E(^5T_2))^2}{4 \cdot E_{NIR}}$			

even if the energy transfer from Mn^{2+} to Mn^{3+} is assumed. The excitation spectra monitored at 617 and 676 nm are the same and no line characteristic for Mn^{2+} appear.

On the other hand, with the very low intensity of the $^1T_2 \rightarrow\ ^5E''$ transition (band at 813 nm) at low temperature in mind, it could be proposed that the bands at 617 nm and 676 nm correspond to the $^1T_2 \rightarrow\ ^5E'$ and $^1T_2 \rightarrow\ ^5E'$ transitions, respectively. However, in this case, the fact that the value of the Jahn–Teller stabilization energy of the $^1T_2$ level decreases greatly (Table 4) indicates that this hypothesis should be rejected. Another possible explanation, commonly called on in spectroscopic studies, is that there are two different Mn^{3+} sites. However, neither the structural data nor the spectroscopic properties of other ions, e.g., Cr^{3+}, support such. The band cannot be described also as the zero-phonon line (ZPL) of the $^1T_2 \rightarrow\ ^5E$ transition; the energy difference between the 674 and 617 nm bands, i.e., 1370 cm^{-1} is too great. The high Mn content of the red beryl opens the possibility of luminescence from Mn^{3+}–Mn^{3+} pairs. However, emission from pairs appears always at longer wavelengths and the luminescence decay is not a single exponential. No additional emission band was observed for the doped garnets of Kück et al. (1998a) with 0.05–0.4 at% Mn^{3+} compared to 0.28 at% in the red beryl. The high Mn content also suggests, though rather questionably, comparison with similar spectra illustrating intra-atomic Mn^{3+} photoluminescence in $YMnO_3$ (Takahaski et al. 2002; Nakayama et al. 2014) and in GaMnN (Zenneck et al. 2007). Any possible interaction of point defects with nearby Mn^{3+} ions is weak; the 617 nm emission band is not seen on the spectrum at 300 K or on the spectrum measured during ultrashort laser excitation.

It was difficult to measure the luminescence spectra of Mn-bearing vesuvianites at room temperature. Purple vesuvianite provided the only good-quality spectrum. Using continuous radiation from a xenon lamp, a wide emission band with maxima at 617 and 660 nm was measured (Fig. 6a). Failure to measure the $^5T_2 \rightarrow\ ^5E''$ emission band expected at 700–800 nm was due to the strong intensity of the excitation source. The width of the 617 nm band is greater (1368 cm^{-1}) than that of the 660 nm band (803 cm^{-1}).

The low temperature (7K) luminescence spectra of purple- and pink vesuvianite from the Jeffrey Mine contain Mn^{3+} emission bands at 657 and 666 nm (Fig. 6a, b). The characteristic luminescence of Cr^{3+} is shown in Fig. 6c. The luminescence of Cr^{3+} corresponds to two R_1 lines at 700 nm (14,278 cm^{-1}) and 694 nm (14,407 cm^{-1}). Only one R_2 line peaked at 688 nm (15,528 cm^{-1}). The intensity ratio of these lines at low temperature (7 K) prevents any other assignment of them. The two R_1 lines indicate that the Cr^{3+} ions occupy two non-equivalent crystal sites.

Hålenius (2000) who showed the presence of Cr^{3+} ions in the octahedral Y3 site also anticipated their presence in the five-fold coordinated C_{4v} (Y1) site. The emission of a green vesuvianite was documented, and the energy levels of the Cr^{3+} ion in the C_{4v} site calculated, by Czaja (2002). As the emission lines at 14,407 and 14,528 cm^{-1} could be identified as R_1 and R_2 lines from the C_{4v} Y1 site (II), the emission from 14,278 cm^{-1} should originate from the Y2,3 site type

Table 4 The Jahn–Teller stabilization energies of excited level $^1T_2$ of studied crystals

Spectroscopicparameters	Crystal			
	Unit	Red beryl		GSGG/YAGa
		Emission at 7 K	Other assumption	
$\lambda_1\ ^1T_2 \rightarrow\ ^5E''$	[nm]	676	617	659/620
E_1	[cm^{-1}]	14,793	16,207	15,167/16,143
$\lambda_2\ ^1T_2 \rightarrow\ ^5E'$	[nm]	813	676	842/758
E_2	[cm^{-1}]	12,300	14,793	11,884/13,199
τ	[μs]	183	–	4334/8150
$\Delta E(^1T_2)$	[cm^{-1}]	2447	1414	3283/2944
$\Delta E_{JT}(^1T_2)$	[cm^{-1}]	226	75	366/301
$\Delta E_{JT}(1T_2) = \frac{(\Delta E(^1T_2))^2}{4 \cdot E_{NIR}}$				

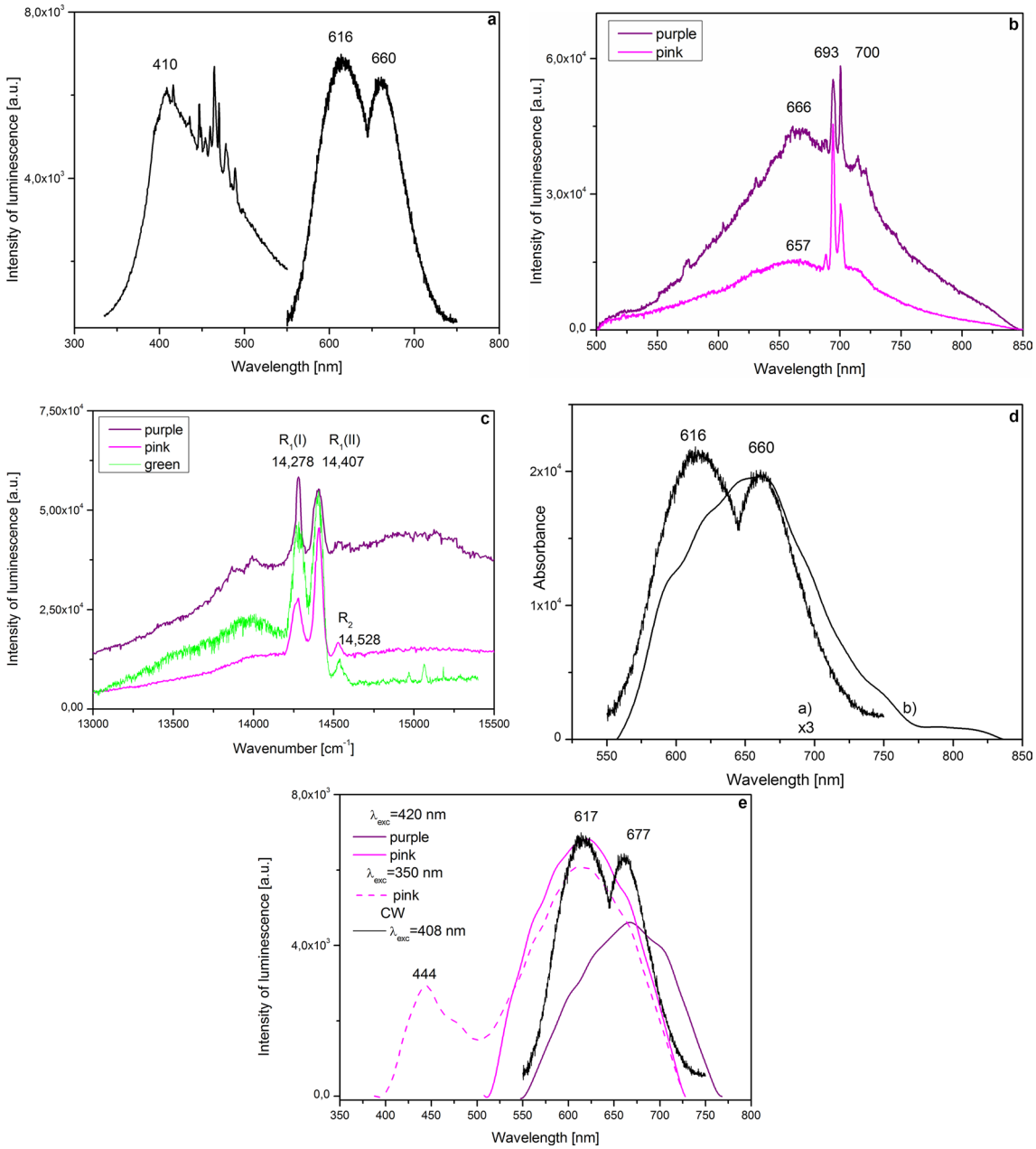

Fig. 6 **a** Room-temperature photoluminescence spectra of vesuvinite: Excitation (left) and emission spectrum (right) measured at $\lambda_{em} = 660$ and 616 nm and $\lambda_{ex} = 410$ nm, respectively. **b** 7 K-temperature emission spectra of pink- and purple vesuvianite variations. **c** 7 K-temperature emission spectra of green-, pink- and purple vesuvianite variations. **d** Emission spectra of vesuvianite without chromium ions: (a) $T = 300$ K, intensity multiplied by factor of 3; (b) $T = 7$ K. **e** Emission of pink- and purple variations of vesuvianite during ultrashort excitations (colored lines) measured at $T = 300$ K compared with room-temperature spectrum under continuous excitation

(I) (Czaja 2002). This site (I) should be identified as a Y2,3s, i.e., a site with symmetry C_{2v} and site (II) as a Y1 five-fold coordinated C_{4v} site. The luminescence lifetime of the R_1-lines was found to be 20 µs. The emission bands of Mn^{3+} measured at room temperature corresponds to the $^5T_2 \rightarrow {}^5E'$ transition, and that measured at low temperature (660 nm) is attributed to the $^1T_2 \rightarrow {}^5E'$ transition. The relative Mn^{3+} to Cr^{3+} luminescence intensity of the purple vesuvianite described here is higher than that of the pink variety. In the purple variety, the Cr^{3+} ions occupy sites (I) and (II) in equal measure. In the pink variety, the Cr^{3+} occupancy of site (I) is much less than that in site (II). If the settlement of the crystal sites by Cr^{3+} and Mn^{3+} is competitive, Mn^{3+} ions should mainly occupy site (I) in the pink vesuvianite.

The emission spectra of another pink vesuvianite not exhibiting Cr^{3+} luminescence were also measured at

room- and low temperatures (Fig. 6d). On the $T = 7$ K spectrum, the band at 620 nm is evident next to that at 658 nm, though not clearly.

With femtosecond excitation, the purple variety of vesuvianite shows only a broad emission band at 677 nm, whereas the pink variety shows broad bands at 617 and 444 nm. The luminescence in the blue spectral range (444 nm) may be associated with point-defect-related emission (Fig. 6e) as its decay time is extremely short (0.4 ns). Decay times of both emission lines at 617 and 677 nm are 0.6 µs and 17 µs at room- and 7K temperatures for both varieties of vesuvianite, with or without Cr^{3+} ions. The short luminescence decay time is due mainly to a high concentration of Mn^{3+} ions.

The origin of the 617 nm emission band in the vesuvianite crystal merits discussion. As for the Mn-bearing beryl, this band is not caused by any other ion according to the excitation spectrum, especially not by Mn^{2+}, as is also shown by the EPR data. For the vesuvianite crystals, it is easier than it is for the beryl to accept that the emission bands 617 and 677 nm reflect Mn^{3+} occupancy of different crystal sites. However, it is not clear why the band at 617 nm disappears at low temperature. On the luminescence spectra of the purple crystal measured under femtosecond excitation, this emission band at 617 nm is also not present; it is in the pink crystal. Thus, it is suggested here that this band is associated with a high Mn-concentration in the pink vesuvianite and, therefore, with an intra-atomic Mn^{3+} photoluminescence or with Mn^{3+}-point defect interaction.

All luminescence decay curves are single exponential and their luminescence lifetimes are short. Thus, the energy transfer among Mn^{3+} ions, or Mn^{3+} and Cr^{3+} ions, or Mn^{3+} and point defects, has mainly a resonance character.

EPR spectra

The main reason for using the EPR method was to establish what proportion of any manganese ions present in the studied crystals was Mn^{2+}. As only an X-band spectrometer was available, no lines of Mn^{3+} were measured due to the very large zero-field splitting energies of this ion.

For many varieties of beryl, EPR axial- and rhombic spectra of Fe^{3+} (Blak et al. 1982b; Gaite et al. 2001; Lin et al. 2013), Ti^{3+} (Bershov 1969; Zheng et al. 2005), Ti^{3+}–Ti^{3+} pairs (Wang and Zheng 2007), Cu^{2+} (Gaite et al. 2001) and CO_2^- and CO_3^- radicals (Anderson 2010) have been presented, as have the spectra of Mn^{2+} in heated purple crystals (Blak et al. 1982a; Gaite et al. 2001) and H^0 (Blak et al. 1982a). In the case of vesuvianite, only the EPR spectrum of Cu^{2+} has been measured and discussed (Dyrek et al. 1992). For a synthetic purple beryl crystal (0.1 Mn wt%), Gaite et al. (2001) measured a single Mn^{2+} sextet line with hyperfine constant $A = 7$ mT. However, on the optical spectrum, the characteristic absorption of Mn^{3+} appeared and the parameter $10D_q = 19{,}000$ cm^{-1} and $B = 700$ cm^{-1} were calculated.

For the red beryl crystal studied by us (0.53 wt%), only a single isotropic line with $g = 1.997$ and a linewidth of 17.68 mT was measured (Fig. 7a). No evidence of the presence of single Mn^{2+} or Mn^{3+} ions, i.e., the well-known sextet of hyperfine lines, was seen. The main reasons for the line broadening are saturation of the spin system, spin–spin interaction and crystal field disorder. The ground states of Mn^{2+} ($^6S_{5/2}$) and of Mn^{3+} (^5E) are very sensitive to the crystal fields of their environment at short- and even long range. As a result, if their environment changes from one to another equivalent position in the structure, the average distribution of the crystal fields will induce a broadening of the transition lines. However, in the beryl crystal studied here, the high concentration of manganese ions makes it prudent to consider whether the origin of the measured resonance line is due to Mn^{2+}–Mn^{2+} or Mn^{3+}–Mn^{3+} interaction, as for rhodonite (Paião and Watanabe 2008). In a low magnetic field, no additional resonance lines appeared.

This line can also be caused by a high iron content. Among the crystals studied by us, 1.47 wt% was the highest amount encountered. When the concentration of the paramagnetic ion exceeds 1%, as it is for Fe, the exchange interaction will yield a characteristic broad absorption curve (Poole and Farach 1972; Marfunin 1979).

Thus, Fig. 7b, c show the EPR spectra of pink- and purple vesuvianite. In low fields, three lines with $g_1 = 6.71$, $g_2 = 5.59$ and $g_3 = 4.46$ have been measured for the pink crystal (Fig. 7b) and only one with $g = 5.93$ for the purple crystal (Fig. 7c). These lines could be recognized as originating from Fe^{3+} impurities. For ferric ions present in tetrahedral coordination and an E/D (rhombicity/axiality) factor of 1/3, the resonance line with $g = \sim 4.28$ is often measured. The other g values were recognized by Hutton and Troup (1964) and Souza et al. (2003) as originating from Fe^{3+} substituting for Al^{3+} in different crystal sites of the kyanite structure. For the allowed transition inside the doublet $-\frac{1}{2} \rightarrow +\frac{1}{2}$ and for $E/D = 0.03$, three resonance lines at 6.71, 5.59 and ~2.00 are expected. For this same transition and $E/D = 0.00$, a resonance line close to 6.0 and a second close to 2.00 may appear. The EPR measurements show that the studied vesuvianite crystals differ in the types of electron defects and in the crystal sites occupied by Fe^{3+} (Castner et al. 1960; Pan and Nilges 2014; SivaRamaiah et al. 2011; van Die et al. 1987). It is concluded that, in the pink vesuvianite, Fe^{3+} is present in two sites, a tetrahedral site when $Fe^{3+} \rightarrow Si^{4+}$ and a second with low symmetry when Fe^{3+} substitutes for Al^{3+} in Y sites. In the purple vesuvianite, the Fe^{3+} ions are present in the site with axial symmetry, most probably Y1 (C_{4v}).

For the pink vesuvianite, a very sharp axial line with $g_{\parallel} = 2.000$, $g_{\perp} = 1.999$ and linewidth 0.4 mT was measured (Fig. 7b). For the purple vesuvianite, an additional isotropic

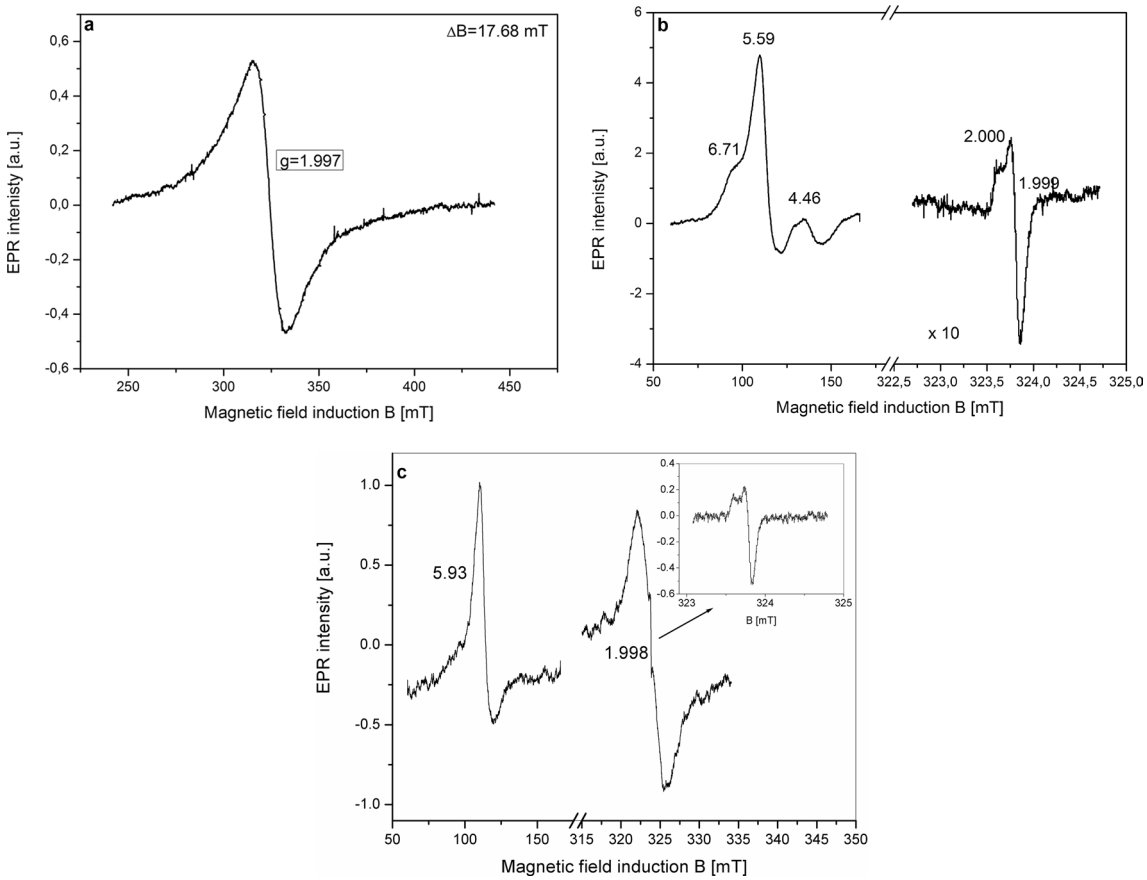

Fig. 7 **a** EPR spectrum of red beryl at 9.0598 GHz and $T = 300$ K. **b** EPR spectra of pink vesuvianite at 9.0599 GHz and $T = 300$ K. **c** EPR spectra of purple vesuvianite at 9.0597 GHz and $T = 300$ K

line with $g = 1.998$ and linewidth 7.7 mT was measured (Fig. 7c), as were two resonance lines (Fig. 7c). The first of these is an intensive isotropic line with $g = 1.998$ and a linewidth of 7.7 mT and the second is the same as for the pink vesuvianite crystal (insert in Fig. 7c). This sharp resonance line could come from electron centers stabilized by trivalent cations, two for purple and one for pink.

In our study, we focused attention on the luminescence properties of Mn^{3+} ion in some minerals. Among the conclusions drawn from the spectroscopic results, some relate to the occupation of lattice sites. These conclusions are not supported by the results of the diffraction studies. X-ray crystallographic methods are the most appropriate for defining crystal site positions and their occupancy by cations. Our intention, however, was to present and discuss luminescence spectra of the Mn^{3+} ion that are so rarely measured for minerals.

Conclusions

The red beryl crystal contains significant Fe, Ti and Zr in addition to Mn. The crystal-field splitting $10D_q = 18{,}250\ cm^{-1}$. The CSFE = 10,950 cm^{-1} and the Jahn–Teller CFSE of the ground level $\Delta E_{JT}(^5E) = 1655\ cm^{-1}$ are the lowest (Tables 2, 3, 4). The short luminescence decay time is most likely caused by a high concentration of Mn in this crystal. The high concentration of the spins is reflected in the wide EPR single isotropic line with $g = 1.997$.

A strongest crystal field ($10D_q = 19{,}380\ cm^{-1}$) was identified for the purple vesuvianite. In addition, the CFSE = 15,043 cm^{-1} and the Jahn–Teller SCFE of the ground level $\Delta E_{JT}(^5E) = 1708\ cm^{-1}$ are higher than for red beryl. It is likely that Mn^{3+} ions are present in sites with C_{4v} symmetry. Fe^{3+} occurs in this site, as can be seen from EPR spectra. Cr^{3+} ions, in some crystals, compete with Mn^{3+} ions to occupy both crystal sites (mainly C_{2v}, and C_{4v}). At room temperature, the emission band at 617 nm, additional to the $^5T_2 \rightarrow {}^5E$ transition at 677 nm, appears. The band at 617 nm may reflect luminescence from intra-atomic transition.

The pink vesuvianite variety is distinguished by its high Mn content. In some pink crystals, Cr^{3+} ions occur, as in some purple vesuvianite. Chromium Cr^{3+} ions are present mainly in tetragonal C_{4v} sites, whereas Fe^{3+} ions substitute for Si^{4+} and occupy C_{2v} sites with rhombohedral symmetry ($E/D \neq 0$). Mn^{3+} ions are also present in C_{2v} sites, it is possible than in Y2 and Y3 sites. For this type of vesuvianite, the following spectral parameters are calculated: $10D_q = 17{,}118\ cm^{-1}$ ($16{,}410\ cm^{-1}$), $CFSE = 13{,}225\ cm^{-1}$ ($12{,}678\ cm^{-1}$) and the Jahn–Teller CFSE of ground level $\Delta E_{JT}(^5E) = 1712\ cm^{-1}$. Among all the crystals studied for the purposes of this paper, the pink vesuvianite had the lowest value of the crystal-field strength (10Dq), but at the same time, it had the highest the Jahn–Teller CFSE level. The high concentration of Mn^{3+} in this pink crystal favors the possibility of intense interactions between Mn^{3+} ions and the presence of other defects in the crystal structure. These defects are revealed by emission lines at 617 nm for both continuous wavelength- and femtosecond-pulse types of excitation, and by the emission band at 444 nm and a very narrow (0.4 mT) axial resonance band on the EPR spectra. The luminescence-decay lifetimes of the $^1T_2 \rightarrow {}^5E\ Mn^{3+}$ transition for both the pink- and purple vesuvianites are shorter than that for red beryl due to the transfer of energy to Cr^{3+} ions.

The emission band measured for the vesuvianite crystal at 617 nm should be a concentration effect. For garnets studied by Kück et al. (1998a), the doping level was from 0.05 to 0.20 at% Mn. Though the Mn at% of the crystals studied by us are 0.28 for the red beryl, 0.41 for the purple vesuvianite and 0.73 for the pink vesuvianite, why no concentration effects are seen on the luminescence decay curves remains unexplained.

Acknowledgements This research project was supported by the Polish National Science Centre (Grant DEC-2011/03/B/ ST10/06320) and by statutory funding from the Faculty of Earth Sciences at the University of Silesia. Dr. Padhraig S. Kennan (University College Dublin, Ireland) is thanked for help with language.

References

Abs-Wurmbach I, Langer K. Tillmanns E (1977) Structure and Polarized Absorption Spectra of Mn^{3+}-substituted Andalusites (Viridines). Naturwisschenschaften 64:527–528

Abu-Eid RM, Langer K, Seifert F (1978) Optical absorption and Moossbauer spectra of purple and green Yoderite, a Kyanite-related mineral. Phys Chem Miner 3:271–289

Anderson LO (2010) EPR investigation of NO_2 and CO_2^- and other radicals in beryl. Phys Chem Miner 37:435–451

Armbruster T, Gnos E (2000) Tetrahedral vacancies and cation ordering in low-temperature Mn-bearing vesuvianites: indication of a hydrogen-like substitution. Am Mineral 85:570–577

Armbruster T, Gnos E, Dixon R, Gutzmer J, Hejny C, Döbelin N, Medenbach O (2000) Manganvesuvianite and tweddelite, two new Mn^{3+}–silicate minerals from the Kalahari manganese field, South Africa. Mineral Mag 66:137–150

Artioli G, Rinaldi R, Stahl K, Zanazzi PF (1993) Structure refinements of beryl by single-crystal neutron and X-ray diffraction. Am Miner 78:762–768

Bershov LV (1969) EPR of Ti^{3+} in beryl. Zh Strukt Khim 10:141–141. https://doi.org/10.1007/BF00751970

Blak AR, Isotani S, Watanabe S (1982a) Optical absorption and electron paramagnetic resonance studies of colorless and pink beryl. Rev Bras Fis 12:285–292

Blak AR, Isotani S, Watanabe S (1982b) Optical absorption and electron paramagnetic resonance in blue and green natural beryl. Phys Chem Miner 8:161–166

Burns RG (1993) Mineralogical applications of crystal field theory. Cambridge

Burns RG, Strens RGJ (1967) Structural interpretation of polarized absorption spectra of the Al–Fe–Mn–Cr epidotes. Mineral Mag 36:204–226

Castner T, Newell GS, Holton WC, Slichter CP (1960) Note on the paramagnetic resonance of iron in glass. J Chem Phys 32:668–673

Chithambo ML, Raymond SG, Calderon T, Townsend (1995) Low temperature luminescence of transition metal-doped beryls. J Afr Earth Sci 20:53–60

Cornu L, Duttine M, Gaudon M, Jubera V (2014) Luminescence switch of Mn-Doped $ZnAl_2O_4$ powder with temperature. J Matter Chem C 2:9512–9522

Czaja M (2002) Luminescencja jonów chromu w naturalnych krzemianach. Polish. Wydawnictwo Uniwesytetu Śląskiego Katowice

Dyrek K, Płatonow AN, Sojka Z, Żabiński W (1992) Optical absorption and EPR study of Cu^{2+} ion in vesuvianite ("cyprine") from Saulan, Telemark, Norway. Eur J Mineral 4:1285–1289

Fitzgerald S, Rheingold AL, Leavens PB (1986) Crystal structure of a non-*P*4/*nnc* vesuvianite from Asbestos. Quebec Am Mineral 71:1483–1488

Fridrichová J, Bačík P, Ertl A, Wildner M, Dekan J, Miglierini M (2017) Jahn–Teller distortion of Mn^{3+}-occupied octahedra in red beryl from Utah indicated by optical spectroscopy. J Mol Struct. https://doi.org/10.1016/j.molstruc.2017.09.081

Gaft M, Nagli L, Panczer G, Rossman GR, Reisfeld R (2011) Laser-induce time-resolved luminescence of orange kyanite Al_2SiO_5. Opt Mater 33:1476–1480

Gaft M, Yeates H, Nagli L, Panczer G (2013) Laser-induced time resolved spectra of natural grossular $Ca_3Al_2(SiO_4)_3$. J Lumin 137:43–53

Gaite J-M, Izotov VV, Nikitin SI, Prosvirnin SY (2001) EPR and optical spectroscopy of impurities in two synthetic beryls. Appl Magn Reson 20:307–315

Ghose S, Kersten M, Langer K, Rossi G, Ungaretti L (1986) Crystal field spectra and Jahn Teller effect of Mn^{3+} in clinopyroxene and clinoamphiboles from India. Phys Chem Miner 13:291–305

Hålenius U (1978) A spectroscopic investigation of manganian andalusite. Can Miner 16:567–575

Hålenius U (1984) The crystal field spectra of Mn^{3+} in chlorite. Geologiska Foreningens i Stockholm Forhandlingar 106(1):51–57

Hålenius U (2000) Optical absorption spectra of Cr-bearing vesuvianite: detection and measurement of Cr^{3+} at octahedral Y3-site. Per Miner 69:35–48

Hålenius U (2004) Stabilization of trivalent Mn in natural tetragonal hydrogarnets on the join "hydrogrossular"-henritermierite, $Ca_3Mn^{3+}{}_2[SiO_4]_2[H_4O_4]$. Mineral Mag 68:335–341

Hålenius U, Skogby H (1996) Crystal field spectra of trivalent manganese in synthetic and natural (Na^{+}–Mn^{3+})-substituted diopside. Eur J Miner 8:1231–1240

Hutton DR, Troup GJ (1964) Paramagnetic resonance of Cr3 + in kyanite. Br J Appl Phys 15:275–280. http://minerals.gps.caltech.edu

Kai AT, Larsson S, Halenius U (1980) The electronic structure and absorption spectrum of MnO_6^{9-} Octahedra in manganian andalusite. Phys Chem Miner 6:77–84

Kück S, Hartung S, Hurling S, Petermann K, Huber G (1998a) Optical transitions in Mn^{3+}-doped garnets. Phys Rev B 57:2203–2216

Kück S, Hartung S, Hurling S, Petermann K, Huber G (1998b) Emission of octahedrally coordinated Mn^{3+} in garnets. Spectrochim Acta Part A 54:1741–1749

Kück S, Hartung S, Hurling S, Petermann K (1998c) Mn^{3+}: fundamental spectroscopy and excited-state absorption. Laser Phys 8:206–209

Langer K, Smith G, Halenius S (1982) Reassignment of the absorption spectra of purple yoderite. Phys Chem Miner 8:143–145

Langer K, Tillmanns E, Kersten M, Almen H, Arni RK (2002) The crystal chemistry of Mn^{3+} in the clino- and orthozosite structure types, $Ca_2M_3^{3+}[OH|O|SiO_4|Si_2O_7]$: a structural and spectroscopic study of some natural piemontites and thulites and their synthetic equivalents. Zeitschrift für Kristallografie 217:563–580

Lin J, Chen N, Huang D, Pan Y (2013) Iron pairs in beryl: new insights from electron paramagnetic resonance, synchrotron X-ray absorption spectroscopy, and ab initio calculations. Am Miner 98(10):1745–1754

Marfunin AN (1979) Spectroscopy, luminescence and radiation centers in minerals. Springer, Berlin

Nakayama M, Furukawa Y, Maeda K, Takeshi Y, Uga H, Fujimura N (2014) Correlation between the intra-atomic Mn^{3+} photoluminescence and antiferromagnetic transition in an $YMnO_3$ epitaxial film. Appl Phys Express 7:023002–023001-023002-04

Nassau K, Wood DL (1968) An examination of red beryl from Utah. Am Miner 53:801–806

Paião JRB, Watanabe S (2008) Thermoluminescence, electron paramagnetic resonance and optical absorption in natural and synthetic rhodonite crystals. Phys Chem Miner 35:535–544

Palanza V, Galli A, Lorenzi R, Moretti F, Mozzati MC, Paleari A, Spinolo G (2010) Luminescence study of transition metal ions in natural magmatic and metamorphic yellow sapphires. IOP Conf Ser Mater Sci Eng 15 (012086). https://doi.org/10.1088/1757-899X/15/1/012086

Pan Y, Nilges MJ (2014) Electron paramagnetic resonance spectroscopy: basic principles, experimental techniques and applications to earth and planetary sciences. Rev Miner Geochem 78:655–690

Panikorovkii TL, Shilovskikh VV, Avdontseva EY, Zolotarev AA, Pekov IV, Britvin SN, Hålenius U, Krivovichev SV (2017) Cyprine, $Ca_{19}Cu^{2+}(Al,MgMn)_{12}Si_{18}O_{69}(OH)_9$, a new vesuvianite-group mineral from the Wessel mine, South Africa. Eur J Miner 29:295–306

Płatonov AN, Żabiński W, Sachanbiński M (1995) Optical absorption spectra of Mn^{3+} ions in vesuvianites from Lower Silesia, Poland. Eur J Miner 7:1345–1352

Poole CP Jr, Farach HA (1972) The theory of magnetic resonance. Wiley, New York

Sugano S, Tanabe Y, Kamimura H (1970) Multiplets of transition metal ion in crystals. Academic, New York

Sherman D, Vergo N (1988) Optical spectrum, site occupancy, and oxidation state of Mn in montmorillonite. Am Miner 73:140–144

SivaRamaiah G, Lin J, Pan Y (2011) Electron paramagnetic resonance spectroscopy of Fe^{3+} ion in amethyst: thermodynamic potentials and magnetic susceptibility. 38: 159–167

Smith G (1978) A reassessment of the role of iron in the 5000–30,000 cm^{-1} region of the electronic absorption spectra of tourmaline. Phys Chem Miner 3:343–373

Smith G. Halenius U, Langer K (1982) Low temperature spectral studies of Mn^{3+}-bearing andalusite and epidote type minerals in the range 30,000–5000 cm^{-1}. Phys Chem Miner 8:136–142

Souza SO, Selvin PC, Watanabe S (2003) Thermally stimulated luminescence, optical absorption and EPR studies in kyanite crystals. J Lumin 102–103:575–580

Powell RC (1998) Physics of solid-state laser materials. Springer, New York

Takahashi J, Kohn K, Hanamura E (2002) Luminescence spectrum from hexagonal $YMnO_3$. J Lumin 100:141–145

van Die A, Leenaers ACHI., der Weg WF, Blasse G (1987) A search for luminescence of the trivalent manganese ion in solid aluminates. Mat Res Bull 22:781–787

Wang F, Zheng WCh (2007) Investigation of EPR parameters for the trigonal Ti^{3+}–Ti^{3+} pair in beryl crystal. Spectrochim Acta A 67:1281–1283

Wood DL, Nassau K (1968) The characterization of beryl and emerald by visible and infrared absorption spectroscopy. Am Miner 53:777–800

Zenneck J, Niermann T, Mai D, Roever M, Kocan M, Malindretos J, Seibt M, Rizzi A (2007) Intra-atomic photoluminescence at 1.41 eV of substitutional Mn in GaMnN of high optical quality. J App Phys 101:063504-063501-063504-3

Zheng W-Ch, Zhou Q, Wu XX, Bei Y (2005) Theoretical investigations of the EPR parameters of Ti^{3+} in Beryl crystal. Z Naturforsch 61a:286–288